ADVANCED MATERIALS INTERFACES
www.advmatinterfaces.de

Self-Stratifying Porous Silicones with Enhanced Liquid Infusion and Protective Skin Layer for Biofouling Prevention

Alex Vena, Stefan Kolle, Shane Stafslien, Joanna Aizenberg, and Philseok Kim**

Liquid-infused silicones are a promising solution for common surface adhesion problems, such as ice accumulation and biofilm formation, yet they generally lack the tunability, mechanical durability and/or longevity essential for industrial applications. Self-stratifying porous silicones (SPS) infused with compatible silicone oil are developed as a passive strategy to address these shortcomings. Through emulsion templating, porosity is formed in the bulk polymer, providing increased free volume for oil infusion, while a non-porous skin layer is formed at the surface. The bulk porosity and pore size distribution of SPS are independently controlled by varying water and surfactant concentration respectively, leading to a higher volume of oil infusion and improved oil retention relative to an unmodified silicone. Despite a higher oil loading and bulk porosity, the skin layer provides liquid-infused SPS with a comparable surface elasticity to liquid-infused silicones. The potential of liquid-infused SPS as a nontoxic fouling release coating for marine applications is demonstrated using laboratory assays against a variety of soft and hard fouling organisms.

1. Introduction

In the past decade, bioinspired liquid-infused surfaces have emerged as a means to solve pervasive sticky problems in households and industry,[1,2] including clothing stains,[3,4] biofilm adhesion on filtration membranes and marine vessels,[5–10] ice accumulation on refrigerator coils, airplanes and windshields,[11–19] as well as bacterial contamination in catheters and other medical devices.[20–29] Liquid-infused surfaces rely on the presence of a stable liquid overlayer to repel various foulants, contingent on the immiscibility of the liquid and impinging foulant. Over time, depletion of the liquid overlayer through various environmental stresses (e.g., shear, evaporation, diffusion, mixing, etc.) compromises the repellency of liquid-infused surfaces.[9,30–32] To maintain the liquid overlayer on infused surfaces, two different strategies are prevalent in the literature—"liquid retention" and "liquid restoration". Using a retention-based strategy, the liquid overlayer is stabilized through a combination of chemical interactions and capillary forces with a roughened, chemically-compatible substrate; liquid-infused surfaces using this strategy are referred to as slippery liquid-infused porous surfaces (SLIPS) and can be directly manufactured on metallic, ceramic, and polymer surfaces.[33] Using a restoration-based strategy, the liquid overlayer is replenished by an internal reservoir of liquid within the bulk material; liquid-infused surfaces using this strategy are referred to as liquid-infused materials and are typically limited to polymers with high affinity for the liquid.[25,34,35] In particular, silicones are a popular candidate for restorative liquid-infused materials in biomedical applications due to their biocompatibility, flexibility, and chemical affinity for low-surface-tension silicone oils.[23,27]

A number of studies have reported the use of oil-infused polydimethylsiloxane (iPDMS) that shows exceptional antifouling capability and long operation, especially when infused postpolymerization.[5,36] While oil-storing capacity and the associated length of antifouling behavior for infused silicone surfaces are poorly understood and require a detailed mechanistic study, several approaches are being considered in parallel to further extend their longevity, such as introducing vasculature,[10] creating surface texture,[16,37] or varying cross-linking density.[38] Howell et al.

A. Vena, S. Kolle, Prof. J. Aizenberg, Dr. P. Kim
Wyss Institute for Biologically Inspired Engineering
Harvard University
Cambridge, MA 02138, USA
E-mail: jaiz@seas.harvard.edu; philseok.kim@wyss.harvard.edu
S. Kolle, Prof. J. Aizenberg, Dr. P. Kim
John A. Paulson School of Engineering and Applied Sciences
Harvard University
Cambridge, MA 02138, USA
S. Stafslien
Department of Coatings and Polymeric Materials
North Dakota State University
Fargo, ND 58102, USA
Prof. J. Aizenberg
Department of Chemistry and Chemical Biology and Kavli Institute for Bionano Science and Technology
Harvard University
Cambridge, MA 02138, USA
The ORCID identification number(s) for the author(s) of this article can be found under https://doi.org/10.1002/admi.202000359.

DOI: 10.1002/admi.202000359

developed silicones with internal vasculature to introduce and store oil, enabling indefinite restoration of the liquid overlayer via diffusion of oil from the vasculature to the surface.[10] A similar strategy was recently applied in liquid-infused polystyrenes.[39] One challenge with creating a vascularized network is application complexity—it cannot be applied as a coating (brushing, spraying, etc.) but requires a carefully designed fabrication process. In addition, an external oil reservoir and pumping system are required for oil restoration, further limiting its applicability. Alternatively, Yeong et al. designed a surface-textured liquid-infused silicone to improve liquid overlayer retention while providing an internal reservoir for liquid restoration.[37] While this approach is promising to extend the longevity of liquid-infused silicones, further effort is needed to create durable microtexture with a scalable fabrication process. An additional drawback is that surface roughness will significantly decrease the repellency against solid foulants (e.g., ice, biofouling) after the liquid overlayer is depleted.[16,17,40] Using a more straightforward approach, Sotiri et al. investigated the tunability and longevity of liquid-infused silicones by varying cross-linking density and silicone oil viscosity.[38] While lower cross-linking density enabled higher oil infusion capacity, it also promoted faster depletion of the liquid overlayer and reduced material stiffness, counteracting the benefits associated with a larger oil reservoir.

Based on the challenges discussed, a simple and scalable strategy is still needed to increase the longevity of liquid-infused silicones without compromising mechanical durability or performance upon liquid depletion. To address this need, we fabricated self-stratifying porous silicones (SPS) using a scalable water-in-oil emulsion templating method, with bulk porosity to control and maximize oil infusion capacity while creating a non-porous surface "skin layer" to retain surface smoothness and stiffness. The effects of water and surfactant concentrations on the porosity, pore size distribution, and skin thickness are investigated, which are then related to the improved oil infusion capacity and surface elasticity of liquid-infused SPS (iSPS). We demonstrate higher dimensional stability of iSPS after liquid infusion, along with improved oil retention in an accelerated aging test when compared to (non-porous) liquid-infused silicones. To show the feasibility of iSPS coatings for biofouling prevention and removal, we discuss their retention and removal properties using model marine organisms. Overall, the results suggest that self-stratifying porous silicones are an attractive strategy for not only improving the longevity of liquid-infused silicones but also for providing additional control and tunability over a range of material properties.

2. Results and Discussion

2.1. Fabrication of iSPS

SPS with closed-cell porosity was fabricated using an emulsion templating approach (**Figure 1**a,b). All chemicals were used as received, with no additional purification or modification. A nonionic surfactant (Pluronic F-127, Sigma) dissolved in DI water and an addition-cure silicone resin (10:1 Sylgard 184, Dow Corning) were combined using planetary centrifugal mixing (ThinkyMixer ARE-310). The formulation was mixed at 2000 rpm for 1 min and 2200 rpm for 1 min to produce a water-in-silicone emulsion with a creamy, homogenized appearance. The emulsion was then poured into a 3D-printed VeroBlue mold ($20 \times 20 \times 2.5$ mm^3) and cured in a 70-psi pressure chamber at 70 °C for 2 h. In practice, the resin can also be cured at ambient pressure using a suitable defoaming agent. The pressure chamber was used solely to minimize air bubble expansion during curing; formulation degassing under vacuum was not possible as it induced macroscopic phase separation of water from silicone. The cured SPS samples, opaque in appearance, were dried in a convection oven at 70 °C for 48 h

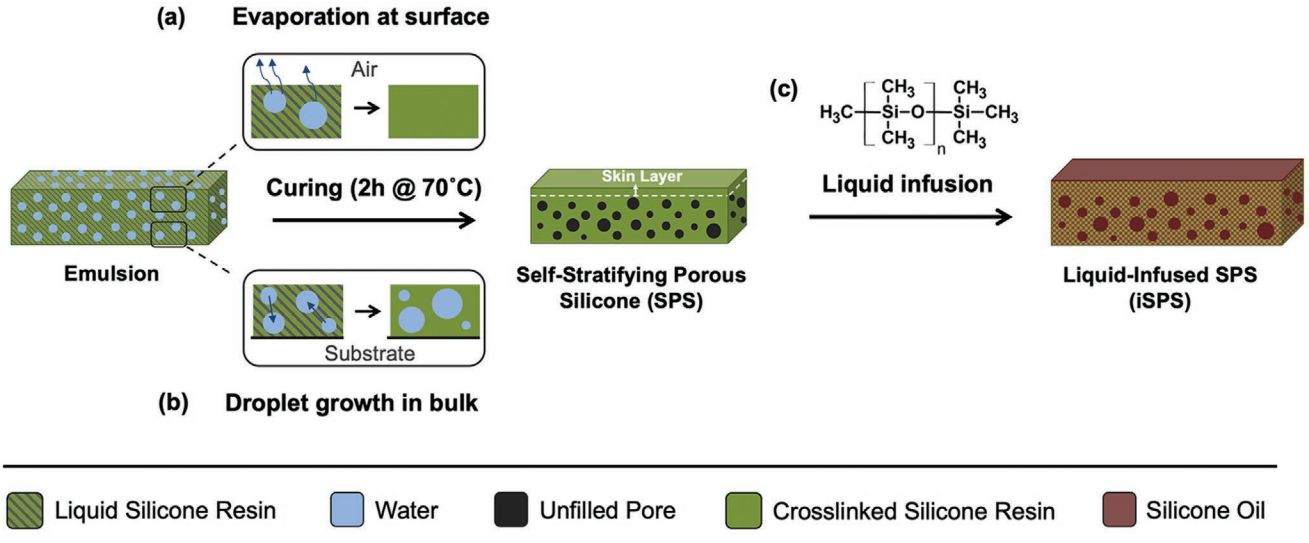

Figure 1. Preparation of liquid-infused self-stratifying porous silicone (SPS) using a water in silicone emulsion. a) Water droplets near the surface evaporate and eventually disappear during the curing process, creating a non-porous skin layer. b) Water droplets in the bulk coalesce/ripen before the polymer has fully cured, leading to a distribution of droplet sizes. Evaporation of water in the bulk continues to occur after the polymer has fully cured, creating a porous microstructure with air voids. c) After curing, SPS is infused with a chemically compatible silicone oil to generate a slippery material, iSPS (liquid-infused SPS).

to remove residual water from the resin. Over 95% of water by mass was removed from SPS samples after oven drying. The mass loss from the SPS samples was attributed to water evaporation as control silicone samples had negligible mass loss under the same drying conditions. Drying the samples for longer periods induced pore collapse,[39,41,42] marked by an increase in sample transparency. The dried resin was then immersed in chemically-compatible methyl-terminated silicone oil (Element14* 10-A, Momentive) until equilibrium oil loading was reached to produce iSPS (Figure 1c).

Multiple SPS variants were prepared to explore the effect of porosity and pore size distribution on silicone oil infusion. SPS samples with different porosities were prepared with a 1 wt% Pluronic solution from 5 to 15 PHR (per hundred resin), while SPS samples with different pore size distributions were prepared with a Pluronic solution (0–10 wt% in water) at 10 PHR. Several SPS samples were formulated with silicone oil (Element14* 10-A, Momentive) in the liquid resin before mixing, which enabled water concentrations as high as 25 PHR (Figure S1a, Supporting Information). Without the addition of silicone oil, the emulsion formed a viscous white paste above 15 PHR with poor self-leveling and cured to form a brittle material with open-cell porosity (Figure S1b, Supporting Information). Viscous emulsions with poor self-leveling have been previously reported for water-in-silicone emulsions at high water concentration, although the reported threshold (70 wt%) was significantly higher than in this study.[43] The established nomenclature in this paper for different (i)SPS samples is (i)SPS-*x*, where *x* represents water content (PHR) in the formulation.

2.2. Characterization of SPS Porosity and Skin Layer

Before liquid infusion, SPS cross-sections were characterized using field emission scanning electron microscopy (FE-SEM) to confirm the presence of porosity in the bulk silicone and a skin layer at the surface. All prepared SPS samples had closed-cell porosity and a non-Gaussian pore size distribution (σ_{avg}), with mean pore diameter (d_{avg}) ranging from 1.65 ± 0.02 to 2.29 ± 0.03 µm. The porosity of SPS was controlled from 0 to 15% by varying water content in the emulsion (**Figure 2**a,b), while the pore size distribution of SPS was predominantly controlled by varying surfactant concentration in water from 0 to 10 wt% (Figure S2a,b, Supporting Information). SPS samples with higher porosity were fabricated when a higher concentration of water was used in the emulsion, while SPS samples with a narrower pore size distribution and smaller mean pore diameter were obtained when a higher concentration of surfactant was used in the emulsion. The water concentration in the emulsion also influenced the pore structure of SPS; pore density, mean pore diameter and pore size distribution increased for SPS prepared with higher water concentrations.

Water droplet dynamics in the emulsion before resin curing can be used to explain the trends in pore size distribution with different water and surfactant concentrations. When the formulation is still in the liquid phase (i.e., during curing but before the resin has cross-linked), higher water concentrations create a reduced mean free path between droplets. A reduced mean free path between droplets promotes droplet growth before the resin has cured by increasing the rate of coalescence and Ostwald

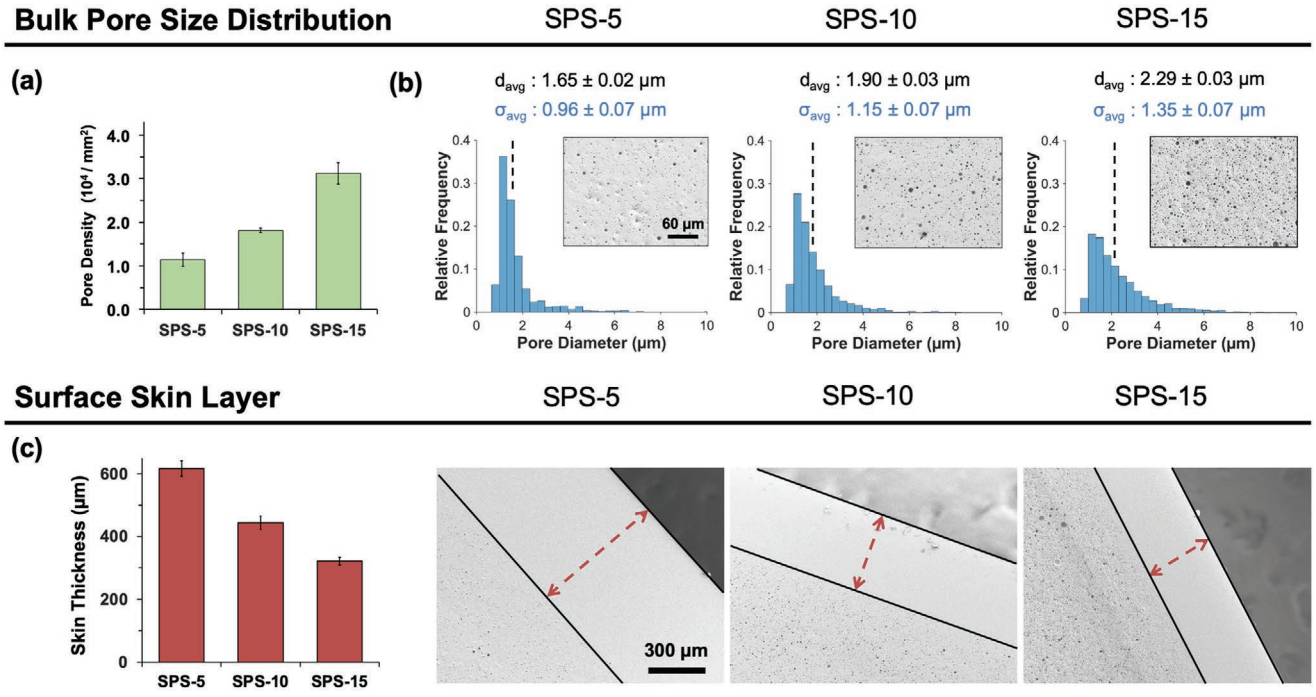

Figure 2. Pore size distribution and skin layer thickness of SPS samples prepared using water concentrations from 5 to 15 PHR in the precursor emulsion [$n = 5$]. a) Bulk pore density in SPS increased linearly with water concentration in the emulsion. b) SEM images and analyzed pore size distribution of bulk porosity in SPS. The mean pore diameter (d_{avg}) and pore size distribution (σ_{avg}) increased with an increase in water concentration in the emulsion. c) Skin layer thickness decreased as water concentration in the emulsion was increased. Vertical cross-sections of SPS samples confirmed the presence of a surface skin layer and the controlled thickness variation using different water concentrations.

ripening, leading to a larger mean droplet size and a broader droplet size distribution in the emulsion. At the same time, higher surfactant concentrations stabilize the water droplets by reducing interfacial energy at the water-silicone interface, which lowers the rate of droplet coalescence and Ostwald ripening before the resin has cured. A lower droplet growth rate leads to a smaller mean droplet size and a narrower droplet size distribution in the emulsion. Overall, the pore sizes and distributions observed for SPS with varying water and surfactant concentrations are in excellent agreement with existing literature on porous silicones.[41,43–45] Interestingly, we were able to prepare metastable water in silicone emulsions with high shear mixing but without any surfactant, which enables a more environmentally friendly approach to fabricate SPS.[43,46] However, as discussed later on, SPS samples prepared without surfactant had lower silicone oil infusion capacity and are less suitable candidates (in their current form) for extending the longevity of iSPS.

Regardless of the controlled variation in porosity and pore size distribution, all SPS samples formed a relatively thick protective skin layer without pronounced voids at the air interface. The skin thickness of SPS decreased from 620 to 250 µm as water concentration (Figure 2c) and surfactant concentration (Figure S2c, Supporting Information) increased in the emulsion. The self-stratification behavior of SPS during curing can be controlled by considering the driving mechanisms of skin layer formation. In general, we found that the skin thickness of SPS is governed by the interplay between the evaporation of water and the curing speed of the SPS mixture (Table S1, Supporting Information). The escape of water molecules from the precured SPS mixture results in the shrinkage and eventual elimination of the emulsified water droplets at the surface of the mixture. If the curing of the SPS mixture is slow enough, the resultant elimination of water droplets can propagate from the surface to deep into the bulk of the mixture and form a thicker skin layer. In the case of either accelerated curing kinetics of the SPS mixture or suppressed evaporation of water from the SPS mixture, the propagation of droplet elimination before curing is restricted, and as a result, a thinner skin layer is observed. For example, a faster silicone curing rate, induced by higher curing temperature or higher curing agent concentrations, restricted the skin layer formation during SPS fabrication. A higher surfactant concentration in water also restricted the skin layer formation by lowering the evaporation rate of water during curing.[47]

Furthermore, skin layer formation is not affected by water droplet sedimentation during curing due to the rather insignificant difference in density between water (ρ_d: 1.00 g cm^{-3}) and liquid Sylgard 184 (ρ_c: 0.98 g cm^{-3}, μ_c: 3.5 Pa s). Stokes law of sedimentation was used to calculate the sedimentation rate (V_{Stokes}) of water droplets in the silicone mixture before curing (Equation (1)).

$$V_{Stokes} = \frac{(\rho_d - \rho_c) g d^2}{18 \mu_c} \quad (1)$$

Stokes Law is generally applied to determine the settling rate of particles in a suspension but is also applicable for calculating the settling rate of discrete droplets in a low concentration emulsion.[48] For 2 µm droplets (d), the sedimentation rate in the mixture is ≈10 pm s^{-1}. Since the mixture cures in less than 2 h at 70 °C, the maximum displacement of a water droplet before curing is 72 nm, which is negligible relative to the droplet's size and the overall material thickness. While the thinnest skin layer measured in this study was 250 µm, there is no theoretical lower bound on skin layer thickness for SPS coatings. By rationally designing SPS curing kinetics relative to water evaporation under relevant application constraints, SPS coatings can be fabricated with arbitrary skin layer thickness relative to coating thickness.

2.3. Characterization of iSPS

After the characterization of porosity and skin layer, the prepared SPS samples (20 × 20 × 2.5 mm^3) were immersed in a silicone oil bath until equilibrium oil infusion was obtained. The equilibrium oil infusion capacity of SPS was determined by removing samples from the silicone oil bath periodically and measuring their mass (after gently removing excess oil on the surface with a Kimwipe) until it plateaued. For this study, oil loading is reported as the mass of infused silicone oil in the cured resin relative to the mass of the cured resin (m_{oil}/m_{resin}). The wetting properties of iSPS were observed by measuring the contact angle hysteresis (CAH) of two liquids immiscible with methyl-terminated silicone oil: water (γ = 72 mN m^{-1}) and ethanol (γ = 22 mN m^{-1}). After infusion with silicone oil, iSPS exhibited significantly reduced CAH: from 28° to 5° for water and from 26° to 5° for ethanol (**Figure 3**). As expected, the bulk porosity of SPS did not have a negative influence on the slippery properties of liquid-infused silicones. There was no significant difference in CAH between iSPS and iPDMS, with both liquid-infused silicones having CAH less than 5°.

All SPS samples had higher oil infusion capacity (hereafter "oil capacity" for short) at equilibrium compared to PDMS (**Figure 4**a). Furthermore, SPS oil capacity increased with

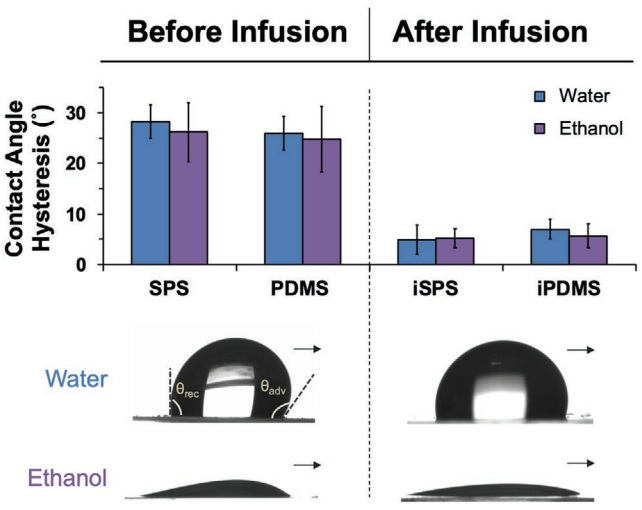

Figure 3. Contact angle hysteresis of two immiscible liquids, water and ethanol, on SPS and PDMS before and after infusion. Sliding droplets had low hysteresis ($\theta_{adv} - \theta_{rec}$ = 5°) on iSPS after silicone oil infusion, comparable to iPDMS [n = 5].

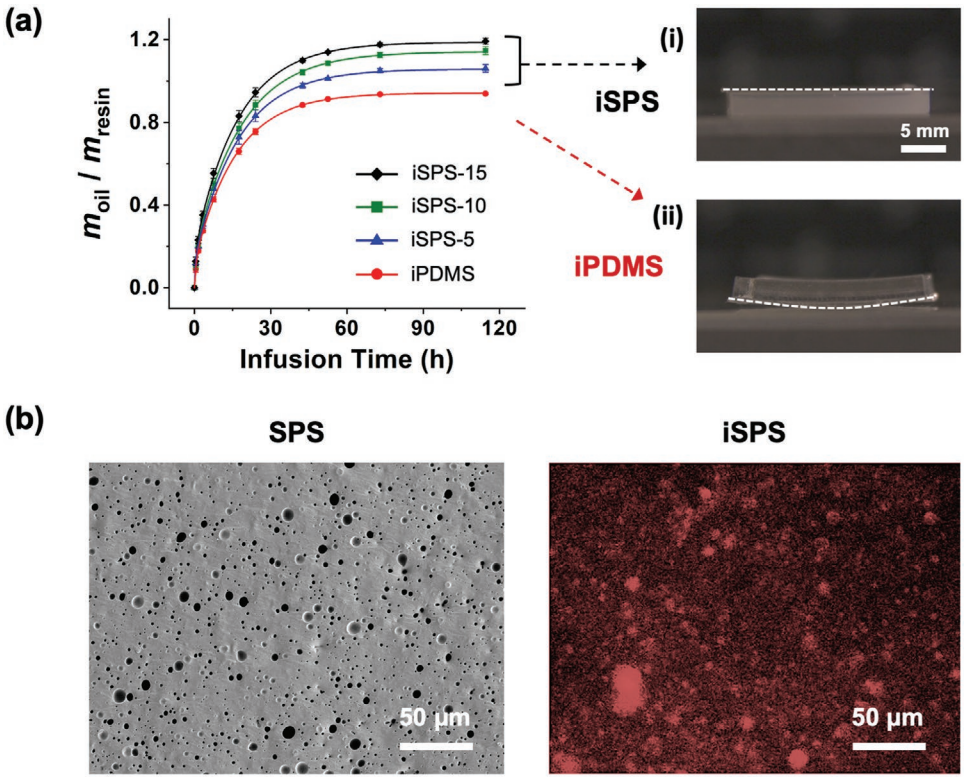

Figure 4. a) Infusion kinetics for SPS immersed in silicone oil, with varying porosity resulting from increased water content [$n = 4$]. Infusion kinetics for non-porous PDMS are also shown as a comparison ("iPDMS"). At equilibrium ($t \approx 120$ h), iSPS had more silicone oil per initial mass of dry resin compared to iPDMS, with a positive correlation between porosity and total infused oil. (i–ii) Photographs of iSPS-15 and iPDMS side profiles after infusion: iSPS maintained its original volumetric proportions while iPDMS deformed significantly during oil infusion. b) SEM image of SPS vertical cross-section before infusion (left), compared to a Z-scan confocal fluorescence image of iSPS vertical cross-section after infusion with PDI-conjugated silicone oil (right). Silicone oil was observed throughout iSPS in the bulk, with high intensity circular fluorescent domains comparably sized to pores observed in SEM images of SPS.

increasing porosity, with iSPS-15 having the highest oil loading of 1.20, compared to 0.94 for iPDMS. To confirm the infusion of pores (i.e., air voids after removal of water) with silicone oil, we evaluated the bulk porosity of iSPS infused with dilute perylenediimide (PDI)-conjugated silicone oil under confocal microscopy. Strong fluorescent circles were observed for samples with a slightly larger size distribution compared to the SPS porosity characterized by SEM (Figure 4b), confirming that the pores in SPS are filled with silicone oil. The experimental data for iSPS infusion is consistent with the theoretical oil capacity of a porous elastomer under isotropic swelling, which results in a proportional increase in pore volume during silicone matrix expansion. When PDMS and SPS materials have comparable cross-linking density, the relationship between iSPS oil capacity (u_{iSPS}) for a given porosity (p) and iPDMS oil capacity (u_{iPDMS}) can be estimated.

$$u_{iSPS} = u_{iPDMS}\,(1+p) + p \tag{2}$$

For $u_{iPDMS} = 0.94$ and $p = 0.15$ (i.e., iSPS-15), the calculated oil capacity is 1.23, which is in good agreement with the observed iSPS-15 oil capacity of 1.20 (Table S2, Supporting Information). A complete derivation of this equation and associated assumptions is included in Equations (S1–S5) (Supporting Information).

In addition to higher oil capacity, iSPS retained its original shape, while iPDMS warped in the later stages of oil infusion (Figure 4a). This result was slightly surprising as iSPS had a higher oil capacity than iPDMS. The warping of iPDMS is attributed to the internal stress built up in the block of silicone due to anisotropic swelling. All square-shaped resins were placed inside a polystyrene petri dish during oil infusion, effectively reducing the diffusion of oil into the resin from the bottom. The improved shape retention of iSPS compared to iPDMS is attributed to its micropores acting as stress relief points (e.g., pore deformation, such as buckling and wrinkling along the interface between the pore and the surrounding resin). The pores in iSPS are effective buffers to mitigate internal stress during silicone oil infusion, which is a promising strategy to avoid delamination when liquid-infused silicones are applied as a coating. Liquid-infused silicones with improved stress relaxation are highly relevant for coating applications since only the outer coating surface will be exposed to silicone oil during infusion. If swelling-induced deformations are too strong, the adhesion between the liquid-infused silicone and the underlying material may fail and lead to coating delamination. Therefore, iSPS is hypothesized to have improved adhesion strength compared to iPDMS for coating applications in general. However, experimental validation is required to determine the magnitude of this improvement on relevant substrates in practical use cases.

Although iSPS-15 has a higher oil capacity than iPDMS, the difference in surface stiffness is minimal: through nanoindentation, the elastic moduli of iSPS-15 and iPDMS were measured to be 300 ± 25 kPa and 345 ± 35 kPa, respectively. Consequently, the iSPS approach can be used to fabricate liquid-infused silicones with higher oil capacity without compromising the surface stiffness. Specifically, this trait can be leveraged to design longer-lasting liquid-infused silicones with reduced attachment of moduli-sensitive organisms.[49,50] The equilibrium oil capacity and elastic modulus of iSPS can be further tuned by varying the surfactant concentration in the formulation (Figure S3, Supporting Information). When the surfactant concentration in water was reduced from 10 to 1 wt% in the emulsion, the oil capacity of iSPS-10 increased from 1.04 to 1.15 (Figure S3a, Supporting Information), which correlated positively with the mean pore diameter (Figure S3b, Supporting Information). Smaller pore diameters (i.e., < 1 µm) are hypothesized to have less infusion as the silicone oil has to overcome a larger Laplace pressure to infiltrate the pores. In this situation, Equation (2) is not valid to estimate the oil capacity of iSPS, as it assumes complete oil infiltration into SPS porosity. As expected, reduced surfactant concentrations in the precursor emulsion increased the elastic modulus of iSPS from 200 to 400 kPa (Figure S3c, Supporting Information), which was directly related to an increase in skin thickness (Figure S3d, Supporting Information).

The restorative ability of liquid-infused polymers has been well documented after liquid overlayer depletion, characterized by diffusion of liquid from the bulk reservoir to the depleted surface.[23,35] The longevity of liquid-infused polymers is directly related to their capability to replenish a depleted liquid overlayer, which improves with higher oil retention.[38] The relative longevity of iSPS samples was investigated by measuring silicone oil retention under artificial aging conditions (**Figure 5**). Although there is no direct correlation between this accelerated method and the actual depletion rate under practical use cases, the accelerated aging experiment still enables a comparison between the relative longevity of iSPS and iPDMS subject to the same mode of failure (i.e., oil depletion). Square samples (1.4 × 1.4 cm^2) were cut out from previously infused silicones of each type to produce test specimens with a consistent surface area. A cured block of PDMS (10:1 Sylgard 184) was then placed on top of the liquid-infused silicone samples, allowing silicone oil to diffuse from the liquid-infused silicone to the dry PDMS (Figure 5a). The volume of the PDMS block was 2× larger than the volume of the liquid-infused samples to better approximate a "perfect sink" for silicone oil. The masses of the liquid-infused silicones were recorded at regular intervals to monitor the loss of silicone oil over time. iSPS started with a higher silicone oil loading than iPDMS (t = 0) but released silicone oil at a similar rate during the first 90 h of accelerated aging (Figure 5b). The cumulative release of silicone oil from liquid-infused silicones was approximately linear when plotted versus $t^{1/2}$, which is consistent with Fickian release kinetics when the short-time approximation is applied.[51] Between 90 and 180 h, iSPS-5 and iSPS-10 continued to release silicone oil at a similar rate, while the rate decreased for iSPS-15. iSPS-15 retained the highest amount of silicone oil after 180 h of accelerated oil release relative to other liquid-infused silicones in the study. Therefore, we anticipate

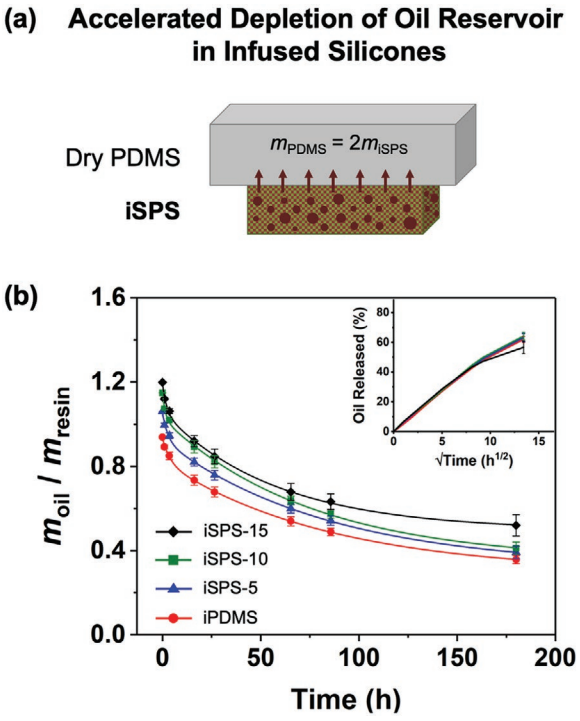

Figure 5. a) Method used to accelerate oil depletion from iSPS samples. A non-infused PDMS resin was cured and placed firmly on top of each infused sample, promoting silicone oil release from iSPS samples over time. b) Accelerated release kinetics of silicone oil from iSPS samples [n = 4]. Inset – Cumulative silicone oil released from samples versus $t^{1/2}$ showing Fickian release kinetics with short time approximation. iSPS-15 retained a higher amount of oil compared to iPDMS, which resulted from a larger oil capacity and a reduced release rate after 90 h of accelerated testing.

that iSPS-15 will maintain its performance for a longer period of time compared to iPDMS.

Overall, iSPS-15 prepared with 1 wt% Pluronic in water was found to be the optimum composition for extended performance longevity of liquid-infused silicones, as the composition had the highest oil capacity and best oil retention in accelerated aging compared to iSPS-10, iSPS-5, and iPDMS. iSPS-15 has higher porosity, larger mean pore size, and a thinner skin layer relative to iSPS-10 and iSPS-5. Since SPS characteristics (i.e., porosity, pore size, skin layer) are interconnected, the relative influence of each structural feature on improved oil retention is challenging to elucidate. As such, a more in-depth mechanistic study with independently controlled features is needed in the future to elucidate the key features that improve oil retention in iSPS coatings.

2.4. Biofouling Mitigation of iSPS for Marine Applications

The biofouling prevention and release characteristics of iSPS-15 were tested against a range of marine fouling organisms to confirm its suitability as a non-fouling coating for marine applications. An initial screening was conducted against a single-cell alga, *Chlamydomonas reinhardtii* (**Figure 6**). After 1 week of static immersion in the algae culture, iSPS was covered in a green, robust biofilm, confirming that the coating was not toxic to the algae. When the samples were slowly withdrawn from

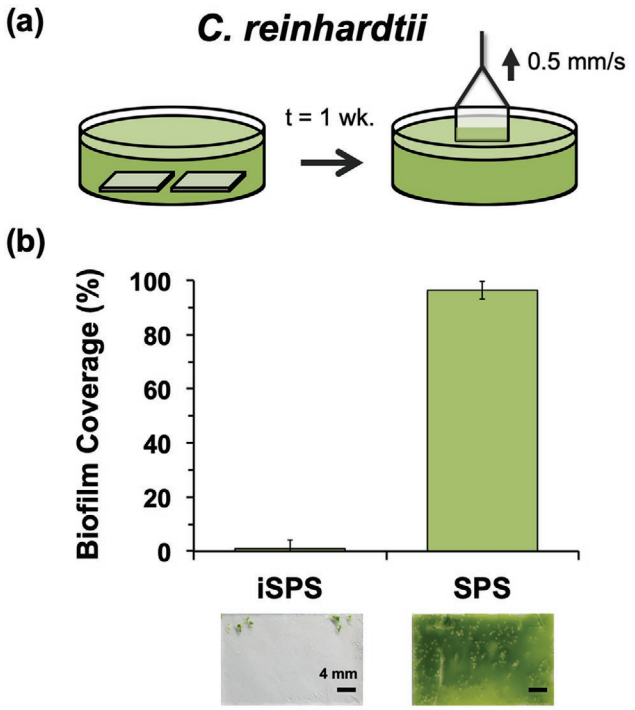

Figure 6. a) Schematic of test used to evaluate biofilm release (*C. reinhardtii*) from iSPS coatings under low-shear conditions. b) Liquid-infused SPS coatings had virtually no biofilm remaining after substrates were removed from the Petri dish at low shear rate. iSPS-15 and SPS-15 formulations were used for testing [$n = 5$].

liquid growth medium, the algal biofilm attached to iSPS was almost completely removed by detachment forces imparted upon the iSPS surface via passage through the air–water interface. In this regard, biofilm retention on iSPS-15 was < 2%, whereas biofilm retention on the dry control SPS-15 was > 95%. The fouling release performance of iSPS matches the performance of liquid-infused PDMS reported in literature,[5] demonstrating that the addition of bulk porosity does not hinder the fouling release properties of liquid-infused silicones.

Porous silicones fabricated with a solid or liquid porogen typically have pores throughout the material, including the solid-air interface.[45,52–54] Surface roughness associated with interfacial porosity decreases biofouling repellency after the liquid overlayer is depleted due to the appearance of a roughened surface presenting new attachment sites.[17] The skin layer approach eliminates interfacial defects associated with surface porosity, which minimizes potential biofouling attachment sites on the coating. In other words, the skin layer enables porous silicones to be fabricated for biofouling applications without compromising performance due to surface porosity.

Following the initial validation of biofouling performance with *C. reinhardtii*, iSPS-15 was tested at North Dakota State University against a broader array of marine fouling species after 7 days of water immersion preconditioning. Preparation and testing of coatings against each organism were conducted using the methodologies established and previously reported by Stafslien et al.[8,55–58] The following controls were also tested: SPS-15, iPDMS, PDMS, PU (polyurethane), and IS900 (Intersleek 900, AkzoNobel, a commercial fouling release coating commonly used as a benchmark). A combination of biofilm-forming microorganisms and hard-fouling organisms were used for testing, including marine bacteria (*Cellulophaga lytica*), diatoms (*Navicula incerta*), mussels (*Geukensia demissa*), and adult barnacles (*Amphibalanus amphitrite*). Additional experimental details are included in the Supporting Information along with statistical analysis of fouling data (Table S3, Supporting Information).

Liquid infusion of SPS substantially reduced biofilm coverage in *C. lytica* retraction testing compared to PDMS, SPS, and PU control treatments (**Figure 7**a). iSPS had comparable biofilm retraction to iPDMS and IS900, which is promising as biofilm retraction has been shown to be a good predictor of the fouling release ability of marine coatings in static ocean immersion testing.[59,60] iSPS also performed exceptionally well against hard-fouling organisms, preventing all mussels from attaching and reducing barnacle reattachment and adhesion to the coating surface (Figure 7b,c). The outstanding performance of iSPS and iPDMS against mussels (i.e., no attachment) is consistent with that of previously reported liquid-infused silicone coatings.[5,61]

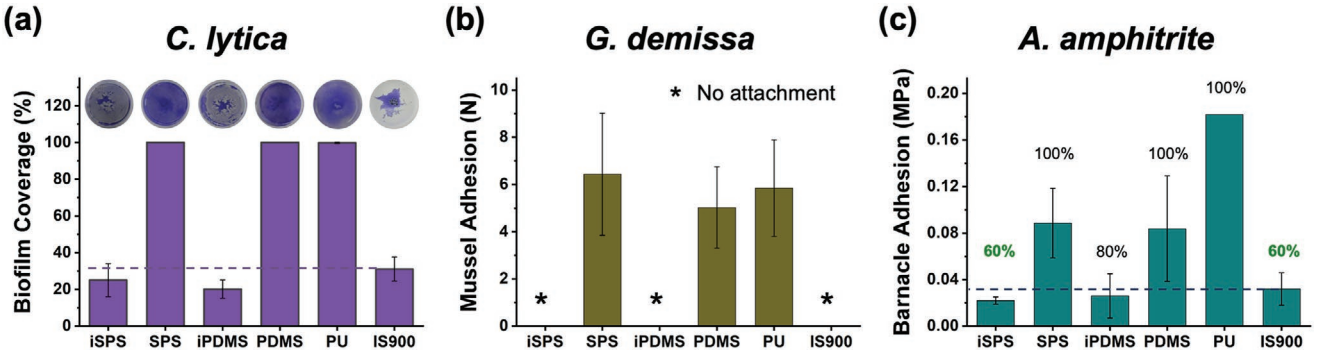

Figure 7. Biological laboratory assays conducted with iSPS and control coatings using model marine fouling organisms. iSPS-15 and SPS-15 formulations were used for testing. For comparison, the performance of a commercial standard Intersleek 900 (IS900) is denoted by a horizontal dashed line. a) Surface coverage of *C. lytica* biofilm after retraction with representative image of biofilm retraction on 2 cm^2 coated coupons [$n = 3$]. b) Mussel attachment and adhesion test with *G. demissa*. Asterisks indicate no mussel attachment [$n = 6$]. c) Adult barnacle reattachment and adhesion test with *A. amphitrite*. The percent values above each average adhesion bar represent the percentage of barnacles that successfully reattached to each coating surface [$n = 5$]. Overall, iSPS had comparable fouling prevention to IS900 against all tested organisms [Error bars = 1σ].

iSPS had lower barnacle reattachment (60%) compared to iPDMS (80%). On the other hand, the adhesion strength of reattached barnacles was comparable for both materials (0.02–0.03 MPa), and 4x lower compared to non-infused silicones with 100% barnacle reattachment. iSPS performance against mussels and barnacles was on par with iPDMS and IS900. The excellent performance of iSPS and iPDMS against barnacles is particularly promising as the reattachment assay correlates well with the prevention and removal of the most problematic hard-fouling organisms that naval vessels and other intermittently used watercraft must combat in the field.[60]

Additional tests with iSPS-15 were conducted against the biofilm-forming microorganisms *C. lytica* and *N. incerta* (Figure S4, Supporting Information). Leachate toxicity tests confirmed that iSPS was nontoxic to both organisms. Surprisingly, leachates extracted from the non-biocidal marine coating Intersleek 900 exhibited toxicity against the diatom *N. incerta*, comparable to the biocidal control solution (Triclosan, Tc, 6 μg mL^{-1}). It should be noted, however, that the coatings were tested after 7 days of water immersion preconditioning and extended durations (i.e., 28 days immersion) typically resolve the toxicity observed for IS900 toward *N. incerta*. Consistent with being a nontoxic coating, liquid infusion of SPS did not markedly reduce *C. lytica* biofilm growth. There was also little impact on *C. lytica* biofilm removal with iSPS, iPDMS, and the non-infused SPS effectively showing the same performance and IS900 showing a small improvement at higher washing pressures (20 psi). The removal efficiency of non-infused SPS is remarkably high. For the *N. incerta* fouling removal assay, the best performance was shown by the PU control for both high and low washing pressures, followed by the performance of iSPS for the low pressure treatment and IS900 for the high pressure treatment. Good performance of iSPS coatings against *N. incerta* is promising as traditional silicone coatings have been reported to perform poorly against this species of diatom.[57] The demonstrated ability of the *C. lytica* and *N. incerta* removal tests to predict the onset and removal of slime films and soft fouling in the field could be of relevance for assessing the grooming performance of these coating systems as well as vetting their potential to alleviate slime fouling on pleasure craft and commercial shipping vessels.[60]

Overall, no significant acute performance differences were observed between iPDMS and iSPS in the biofouling assays (Table S3, Supporting Information). Both materials present a liquid overlayer with comparable reduction in contact angle hysteresis relative to non-infused controls (Figure 3). The controlled formation of a skin layer during SPS curing enables iSPS to provide a smooth PDMS surface without the detrimental effect of pore-induced surface roughness. The extended biofouling longevity of iSPS (due to 30% higher oil infusion and improved oil retention) versus iPDMS is not expected to be fully characterized by acute fouling tests, but rather by long-term field testing in relevant oceanic conditions. Future studies are therefore necessary to validate the long-term performance enhancement of iSPS that are provided by demonstrable improvements in oil infusion capacity and oil retention compared to iPDMS.

While the acute biofouling performance results for liquid-infused silicones (iSPS and iPDMS) were not significantly different from the commercial product IS900, liquid-infused silicones have demonstrated improvements in performance over traditional marine products at several field test sites.[36] Given that this is a comparison between initial prototypes (iSPS, iPDMS) and a fully developed commercial product (IS900), liquid-infusion of silicones remains a promising strategy to improve the performance of antifouling products with further development efforts.

3. Conclusions

In this study, we have demonstrated that self-stratifying porous silicones can be engineered in a one-step, scalable process using emulsion templating to form a porous bulk and a non-porous skin layer. By controlling water and surfactant concentrations in the precursor emulsion, the bulk porosity, pore size distribution, and the skin thickness of SPS can be controlled, which provides additional levers to tune the properties of liquid-infused silicones. SPS has higher silicone oil infusion and retention, as well as improved dimensional stability after infusion compared to (non-porous) PDMS. At the same time, liquid-infused SPS maintains surface stiffness due to controlled formation of a skin layer, while retaining the non-fouling properties of liquid-infused silicones against a variety of marine fouling organisms. As a result, liquid-infused SPS is a promising candidate to extend the lifetime of the liquid overlayer without compromising the durability of liquid-infused silicones. At the same time, further study of liquid-infused SPS is required to validate the long-term biofouling performance through field testing and better understand the mechanisms governing oil infusion and replenishment under relevant application conditions.

To the best of our knowledge, the formation and control of a skin layer at the surface of porous silicones has not been previously reported. Self-stratifying porous materials are an attractive strategy for biofouling control, biomedical, and anti-icing applications, as skin layer formation allows porous materials to retain a smooth surface (to minimize foulant adhesion) without compromising surface durability. The general principles for controlling skin layer formation demonstrated in this work can be used to guide the development of self-stratifying porous materials with other silicone curing chemistries (i.e., condensation, UV). More broadly, the governing principles of skin layer formation discussed in this paper can be applied to other immiscible solvents in a variety of resin systems (particularly elastomers and thermosets), enabling tunability of skin formation in application-relevant curing environments. The simple fabrication process introduced in this paper can accelerate new research and development of self-stratifying porous materials to further optimize their tunability and functionality for different applications, including marine hulls, underwater structures, and medical devices.

4. Experimental Section

Cross-Section Imaging: The skin layer and pore size distribution of SPS was observed using FE-SEM (Zeiss Supra 55VP or Zeiss Ultra Plus). Vertical cross-sections were cut from 20 × 20 × 2.5 mm^3 samples with a razor blade and mounted on SEM stubs using conductive carbon tape. The mounted samples were sputter coated with ≈5 nm of Au to

reduce charging effects (EMS 300T D Dual Head Sputter Coater). All images were taken with an acceleration voltage of 5 keV and recorded using type II secondary electrons (SE2). Skin thickness was measured as the vertical distance between the surface and the onset of bulk porosity [$n = 5$].

Pore Image Analysis: The pore size distribution in the bulk phase of SPS samples was analyzed from SEM images ($300 \times 225\ \mu m^2$, resolution: 2048×1536) using MATLAB 2019. SEM images were converted into binary images using the built-in function *imbinarize* (Otsu's threshold method). The binary images were filtered using the built-in function *bwareaopen* to eliminate small artificial features created by thresholding ($<< 1\ \mu m$). The filtered images were corrected using the built-in function *imclose* (disc, $r = 0.4\ \mu m$) to minimize noise near the pore-silicone interface, and the built-in function *imclearborder* to remove partial pores from the edges of the image. The final processed images were evaluated using the built-in function *regionprops*, which created an array with the area and equivalent diameter of each pore (i.e., the diameter of a circle with equivalent area). A pore size histogram was generated using the equivalent diameters, and the mean (d) and standard deviation (σ) were calculated for each histogram. Sampling statistics (d, σ) obtained from each image were then averaged with replicates [$n = 5$] to estimate population statistics (d_{avg}, σ_{avg}).

Wetting Properties: The wetting properties of samples were evaluated with a Krűss goniometer (Drop Shape Analysis System 100) and corresponding software (DSAS4). Contact angle hysteresis of 8 µL water and ethanol droplets was measured using the tilting method.[62] The built-in tangential regression model ("Tangent 2") was used to measure the advancing contact angle (θ_{adv}) and receding contact angle (θ_{rec}) of droplets [$n = 5$]. The resolution of angle measurements was 0.01°.

Liquid Infusion of Porosity: The infusion of silicone oil in the bulk porosity of SPS was measured using confocal microscopy (Zeiss, LSM 700). SPS-10 was infused for 48 h with 2 wt% PDI-conjugated silicone oil, diluted in M-10A silicone oil. Vertical cross-sections were cut from iSPS-10 with a razor blade and mounted on the specimen stage for analysis. Synthesis of the PDI-conjugated silicone oil and additional method details were previously reported by Cui et al.[35]

Nanoindentation: Mechanical testing was conducted using nanoindentation (U9820A Agilent Nano Indenter G200). A cylindrical flat punch (100 µm diameter) was used to evaluate the storage and loss modulus by measuring the oscillatory response of the surface at 10 Hz, using a 2 µm precompression distance. Three different samples were tested per formulation [$n = 3$]. For each sample, measurements were collected in a 3-by-3 array ($450 \times 450\ \mu m^2$). Due to the high elasticity of the substrates, the loss modulus was negligible for all substrates.

Biofilm Retraction Test (C. reinhardtii): Glass substrates (2 in. × 3 in.) were spin-coated with SPS-15 at 300 rpm for 10 s, followed by 2000 rpm for 20 s, and then cured in a 70 °C oven for 2 h [$n = 3$]. The cured substrates were immersed in silicone oil for 48 h to reach lubricant saturation. Three SPS treatments were left dry as a control. The green alga *C. reinhardtii* (UTEX number 89) from the University of Texas Culture Collection was used as a model organism to explore the biofilm retention on iSPS coatings. *C. reinhardtii* was grown in a soil extract (Bristol medium based) solution under non-axenic conditions for a period of 7 days until maximum cell density was reached. The stock culture was then diluted with fresh soil extract to a 1:5 ratio (stock culture to fresh medium). The diluted culture was added to 80 mL square Petri dishes, containing either liquid-infused SPS or control substrates, allowing the algae to settle on test surfaces. The Petri dishes were then placed under a Sun Blaze T5HO fluorescent light fixture (Sunlight Supply, Inc., Vancouver, WA) and grown under a 16:8 h light-dark cycle at 24 °C for 7 days. After 7 days, the samples were lifted out of the culture medium at a controlled rate of 0.5 mm s^{-1} using a UMP3 syringe pump (World Precision Instruments Inc., USA) to simulate gentle shear stress. The treated substrates were immediately photographed after removal from culture to avoid subsequent biofilm retractions. The photos were then analyzed using ImageJ software to assess the total remaining biofilm coverage after the air–water interface transition.

Statistical Analysis of Fouling Assays: The statistical analysis was conducted with the GraphPad Prism 8.0.2 package. Before analysis, the *C. lytica* biofilm retraction percentage data were transformed using an arcsine transformation. The *G. demissa* and *A. amphitrite* adhesion data were transformed with a double square root transformation. The data sets were analyzed with a one-way ANOVA model after checking for homogeneity of variance using a Brown–Forsyth test. Tukey's honestly significant difference test was conducted as the multiple comparison procedure. All results are reported at the $p < 0.05$ significance level.

Supporting Information

Supporting Information is available from the Wiley Online Library or from the author.

Acknowledgements

This work was funded by the Office of Naval Research (ONR), U.S. Department of Defense, under Award Nos. N00014-17-1-2913 and N00014-12-1-0641. Special thanks go to Dr. Jiaxi Cui for the synthesis of PDI-conjugated silicone oil, Dr. James C. Weaver for the fabrication of 3D-printed molds, Jack Alvarenga for assistance with nanoindentation, Dr. Daniel Rittschof and Beatriz Orihuela of the Duke University Marine Laboratory for supplying barnacles and mussels for biofouling studies, Amos Meeks for deriving the theoretical oil capacity of porous silicones, as well as Gurminder Paink, Ute Thiermann, Fahim Naheem, and Onyemaechi Ahanotu for insightful discussions. This work was performed in part at the Center for Nanoscale Systems (CNS), a member of the National Nanotechnology Infrastructure Network (NNIN), which is supported by the National Science Foundation under NSF Award No. ECS-0335765. CNS is part of Harvard University. The manuscript was written through the contributions of all authors. All authors have given approval to the final version of the manuscript.

Conflict of Interest

Joanna Aizenberg and Philseok Kim are co-founders of Adaptive Surface Technologies, Inc. (AST), and Alex Vena is currently employed by AST.

Keywords

antifouling, liquid-infused coatings, longevity, porosity, silicones

Received: February 27, 2020
Revised: April 11, 2020
Published online:

[1] J. Li, E. Ueda, D. Paulssen, P. A. Levkin, *Adv. Funct. Mater.* **2019**, *29*, 1802317.
[2] M. Villegas, Y. Zhang, N. Abu Jarad, L. Soleymani, T. F. Didar, *ACS Nano* **2019**, *13*, 8517.
[3] C. Shillingford, N. MacCallum, T.-S. Wong, P. Kim, J. Aizenberg, *Nanotechnology* **2014**, *25*, 014019.
[4] V. G. Damle, A. Tummala, S. Chandrashekar, C. Kido, A. Roopesh, X. Sun, K. Doudrick, J. Chinn, J. R. Lee, T. P. Burgin, K. Rykaczewski, *ACS Appl. Mater. Interfaces* **2015**, *7*, 4224.
[5] S. Amini, S. Kolle, L. Petrone, O. Ahanotu, S. Sunny, C. N. Sutanto, S. Hoon, L. Cohen, J. C. Weaver, J. Aizenberg, N. Vogel, A. Miserez, *Science* **2017**, *357*, 668.

[6] L. Xiao, J. Li, S. Mieszkin, A. Di Fino, A. S. Clare, M. E. Callow, J. A. Callow, M. Grunze, A. Rosenhahn, P. A. Levkin, *ACS Appl. Mater. Interfaces* **2013**, *5*, 10074.
[7] H. Bazyar, P. Lv, J. A. Wood, S. Porada, D. Lohse, R. G. H. Lammertink, *Soft Matter* **2018**, *14*, 1780.
[8] T. P. Galhenage, D. Hoffman, S. D. Silbert, S. J. Stafslien, J. Daniels, T. Miljkovic, J. A. Finlay, S. C. Franco, A. S. Clare, B. T. Nedved, M. G. Hadfield, D. E. Wendt, G. Waltz, L. Brewer, S. L. M. Teo, C.-S. Lim, D. C. Webster, *ACS Appl. Mater. Interfaces* **2016**, *8*, 29025.
[9] C. S. Ware, T. Smith-Palmer, S. Peppou-Chapman, L. R. J. Scarratt, E. M. Humphries, D. Balzer, C. Neto, *ACS Appl. Mater. Interfaces* **2018**, *10*, 4173.
[10] C. Howell, T. L. Vu, J. J. Lin, S. Kolle, N. Juthani, E. Watson, J. C. Weaver, J. Alvarenga, J. Aizenberg, *ACS Appl. Mater. Interfaces* **2014**, *6*, 13299.
[11] P. Kim, T.-S. Wong, J. Alvarenga, M. J. Kreder, W. E. Adorno-Martinez, J. Aizenberg, *ACS Nano* **2012**, *6*, 6569.
[12] M. J. Kreder, J. Alvarenga, P. Kim, J. Aizenberg, *Nat. Rev. Mater.* **2016**, *1*, 15003.
[13] K. Golovin, A. Tuteja, *Sci. Adv.* **2017**, *3*, e1701617.
[14] K. Golovin, S. P. R. Kobaku, D. H. Lee, E. T. DiLoreto, J. M. Mabry, A. Tuteja, *Sci. Adv.* **2016**, *2*, e1501496.
[15] L. Zhu, J. Xue, Y. Wang, Q. Chen, J. Ding, Q. Wang, *ACS Appl. Mater. Interfaces* **2013**, *5*, 4053.
[16] Q. Liu, Y. Yang, M. Huang, Y. Zhou, Y. Liu, X. Liang, *Appl. Surf. Sci.* **2015**, *346*, 68.
[17] Y. Zhuo, F. Wang, S. Xiao, J. He, Z. Zhang, *ACS Omega* **2018**, *3*, 10139.
[18] C. Zhang, Y. Xia, H. Zhang, N. S. Zacharia, *ACS Appl. Mater. Interfaces* **2018**, *10*, 5892.
[19] J. H. Kim, M. J. Kim, B. Lee, J. M. Chun, V. Patil, Y.-S. Kim, *Appl. Surf. Sci.* **2020**, *512*, 145728.
[20] A. K. Epstein, T.-S. Wong, R. A. Belisle, E. M. Boggs, J. Aizenberg, *Proc. Natl. Acad. Sci. USA* **2012**, *109*, 13182.
[21] D. C. Leslie, A. Waterhouse, J. B. Berthet, T. M. Valentin, A. L. Watters, A. Jain, P. Kim, B. D. Hatton, A. Nedder, K. Donovan, E. H. Super, C. Howell, C. P. Johnson, T. L. Vu, D. E. Bolgen, S. Rifai, A. R. Hansen, M. Aizenberg, M. Super, J. Aizenberg, D. E. Ingber, *Nat. Biotechnol.* **2014**, *32*, 1134.
[22] Y. Kovalenko, I. Sotiri, J. V. I. Timonen, J. C. Overton, G. Holmes, J. Aizenberg, C. Howell, *Adv. Healthcare Mater.* **2017**, *6*, 1600948.
[23] N. MacCallum, C. Howell, P. Kim, D. Sun, R. Friedlander, J. Ranisau, O. Ahanotu, J. J. Lin, A. Vena, B. Hatton, T.-S. Wong, J. Aizenberg, *ACS Biomater. Sci. Eng.* **2015**, *1*, 43.
[24] J. Li, T. Kleintschek, A. Rieder, Y. Cheng, T. Baumbach, U. Obst, T. Schwartz, P. A. Levkin, *ACS Appl. Mater. Interfaces* **2013**, *5*, 6704.
[25] X. Yao, S. S. Dunn, P. Kim, M. Duffy, J. Alvarenga, J. Aizenberg, *Angew. Chem., Int. Ed.* **2014**, *53*, 4418.
[26] J. Chen, C. Howell, C. A. Haller, M. S. Patel, P. Ayala, K. A. Moravec, E. Dai, L. Liu, I. Sotiri, M. Aizenberg, J. Aizenberg, E. L. Chaikof, *Biomaterials* **2017**, *113*, 80.
[27] C. Howell, A. Grinthal, S. Sunny, M. Aizenberg, J. Aizenberg, *Adv. Mater.* **2018**, *30*, 1802724.
[28] W. He, P. Liu, J. Zhang, X. Yao, *Chem. – Eur. J.* **2018**, *24*, 14864.
[29] G. Mackie, L. Gao, S. Yau, D. C. Leslie, A. Waterhouse, *Trends Biotechnol.* **2019**, *37*, 268.
[30] J. S. Wexler, I. Jacobi, H. A. Stone, *Phys. Rev. Lett.* **2015**, *114*, 168301.
[31] L. R. J. Scarratt, L. Zhu, C. Neto, *Langmuir* **2019**, *35*, 2976.
[32] M. J. Kreder, D. Daniel, A. Tetreault, Z. Cao, B. Lemaire, J. V. I. Timonen, J. Aizenberg, *Phys. Rev. X* **2018**, *8*, 031053.
[33] T.-S. Wong, S. H. Kang, S. K. Y. Tang, E. J. Smythe, B. D. Hatton, A. Grinthal, J. Aizenberg, *Nature* **2011**, *477*, 443.
[34] X. Yao, Y. Hu, A. Grinthal, T.-S. Wong, L. Mahadevan, J. Aizenberg, *Nat. Mater.* **2013**, *12*, 529.
[35] J. Cui, D. Daniel, A. Grinthal, K. Lin, J. Aizenberg, *Nat. Mater.* **2015**, *14*, 790.
[36] S. Kolle, A. Meeks, O. Ahanotu, S. Stafslien, E. Maldonado, L. Vanderwal, J. Weaver, P. Kim, L. Cohen, M. Kreder, L. C. Sing, D. Slocum, K. Hunsucker, S. Teo, J. Aizenberg, *Lubricant-Infused Silicone Elastomers as an Improved Antifouling Marine Coating*, in preparation.
[37] Y. H. Yeong, C. Wang, K. J. Wynne, M. C. Gupta, *ACS Appl. Mater. Interfaces* **2016**, *8*, 32050.
[38] I. Sotiri, A. Tajik, Y. Lai, C. T. Zhang, Y. Kovalenko, C. R. Nemr, H. Ledoux, J. Alvarenga, E. Johnson, H. S. Patanwala, J. V. I. Timonen, Y. Hu, J. Aizenberg, C. Howell, *Biointerphases* **2018**, *13*, 06D401.
[39] D. Zhang, Y. Xia, X. Chen, S. Shi, L. Lei, *Langmuir* **2019**, *35*, 8276.
[40] J. Chen, J. Liu, M. He, K. Li, D. Cui, Q. Zhang, X. Zeng, Y. Zhang, J. Wang, Y. Song, *Appl. Phys. Lett.* **2012**, *101*, 111603.
[41] A. Kovalenko, K. Zimny, B. Mascaro, T. Brunet, O. Mondain-Monval, *Soft Matter* **2016**, *12*, 5154.
[42] R. B. Diego, J. L. G. Ribelles, M. S. Sánchez, *J. Appl. Polym. Sci.* **2007**, *104*, 1475.
[43] A. Davis, S. Surdo, G. Caputo, I. S. Bayer, A. Athanassiou, *ACS Appl. Mater. Interfaces* **2018**, *10*, 2907.
[44] S. Peng, P. G. Hartley, T. C. Hughes, Q. Guo, *Soft Matter* **2012**, *8*, 10493.
[45] J. Zhao, G. Luo, J. Wu, H. Xia, *ACS Appl. Mater. Interfaces* **2013**, *5*, 2040.
[46] M. Juchniewicz, D. Stadnik, K. Biesiada, A. Olszyna, M. Chudy, Z. Brzozka, A. Dybko, *Sens. Actuators, B* **2007**, *126*, 68.
[47] I. White, *Ind. Eng. Chem. Fundam.* **1976**, *15*, 53.
[48] F. Goodarzi, S. Zendehboudi, *Can. J. Chem. Eng.* **2019**, *97*, 281.
[49] M. K. Chaudhury, J. A. Finlay, J. Y. Chung, M. E. Callow, J. A. Callow, *Biofouling* **2005**, *21*, 41.
[50] F. Song, D. Ren, *Langmuir* **2014**, *30*, 10354.
[51] P. L. Ritger, N. A. Peppas, *J. Controlled Release* **1987**, *5*, 23.
[52] D. Zhu, S. Handschuh-Wang, X. Zhou, *J. Mater. Chem. A* **2017**, *5*, 16467.
[53] P. K. Yuen, H. Su, V. N. Goral, K. A. Fink, *Lab Chip* **2011**, *11*, 1541.
[54] S.-J. Choi, T.-H. Kwon, H. Im, D.-I. Moon, D. J. Baek, M.-L. Seol, J. P. Duarte, Y.-K. Choi, *ACS Appl. Mater. Interfaces* **2011**, *3*, 4552.
[55] S. J. Stafslien, J. Bahr, J. Daniels, D. A. Christianson, B. J. Chisholm, *J. Adhes. Sci. Technol.* **2011**, *25*, 2239.
[56] S. Stafslien, J. Daniels, J. Bahr, B. Chisholm, A. Ekin, D. Webster, B. Orihuela, D. Rittschof, *J. Coat. Technol. Res.* **2012**, *9*, 651.
[57] D. C. Webster, B. J. Chisholm, S. J. Stafslien, *Biofouling* **2007**, *23*, 179.
[58] J. R. Burkett, J. L. Wojtas, J. L. Cloud, J. J. Wilker, *J. Adhes.* **2009**, *85*, 601.
[59] S. Stafslien, J. Daniels, B. Mayo, D. Christianson, B. Chisholm, A. Ekin, D. Webster, G. Swain, *Biofouling* **2007**, *23*, 45.
[60] S. J. Stafslien, S. Sommer, D. C. Webster, R. Bodkhe, R. Pieper, J. Daniels, L. Vander Wal, M. C. Callow, J. A. Callow, E. Ralston, G. Swain, L. Brewer, D. Wendt, G. H. Dickinson, C.-S. Lim, S. L.-M. Teo, *Biofouling* **2016**, *32*, 949.
[61] K. M. Kimmins, B. D. James, M.-T. Nguyen, B. D. Hatton, E. D. Sone, *ACS Appl. Bio Mater.* **2019**, *2*, 5841.
[62] H. B. Eral, D. J. C. M. Mannetje, J. M. Oh, *Colloid Polym. Sci.* **2013**, *291*, 247.